The Astrophysical Journal, 794:30 (9pp), 2014 October 10 doi:10.1088/0004-637X/794/1/30

THE QUANTUM INTERFERENCE EFFECTS IN THE SC II 4247 Å LINE OF THE SECOND SOLAR SPECTRUM

H. N. Smitha[1], K. N. Nagendra[1], J. O. Stenflo[2,3], M. Bianda[3], and R. Ramelli[3]
[1] Indian Institute of Astrophysics, Koramangala, Bangalore 560034, India; smithahn@iiap.res.in, knn@iiap.res.in
[2] Institute of Astronomy, ETH Zurich, CH-8093 Zurich, Switzerland; stenflo@astro.phys.ethz.ch, mbianda@irsol.ch
[3] Istituto Ricerche Solari Locarno, Via Patocchi, 6605 Locarno-Monti, Switzerland; ramelli@irsol.ch
Received 2014 April 22; accepted 2014 August 18; published 2014 September 22

ABSTRACT

The Sc II 4247 Å line formed in the chromosphere is one of the lines well known, like the Na I D_2 and Ba II D_2, for its prominent triple-peak structure in Q/I and the underlying quantum interference effects governing it. In this paper, we try to study the nature of this triple-peak structure using the theory of F-state interference including the effects of partial frequency redistribution (PRD) and radiative transfer (RT). We compare our results with the observations taken in a quiet region near the solar limb. In spite of accounting for PRD and RT effects, it has not been possible to reproduce the observed triple-peak structure in Q/I. While the two wing PRD peaks (on either side of central peak) and the near wing continuum can be reproduced, the central peak is completely suppressed by the enhanced depolarization resulting from the hyperfine structure splitting. This suppression remains for all the tested widely different one-dimensional model atmospheres or for any multi-component combinations of them. While multidimensional RT effects may improve the fit to the intensity profiles, they do not appear capable of explaining the enigmatic central Q/I peak. This leads us to suspect that some aspect of quantum physics is missing.

Key words: line: profiles – methods: numerical – polarization – radiative transfer – scattering – Sun: atmosphere

1. INTRODUCTION

With the advent of highly sensitive spectropolarimeters like the Zurich Imaging Polarimeter (ZIMPOL), we now have access to the linearly polarized spectrum of the Sun which is due to coherent scattering processes in the Sun's atmosphere (and which has nothing to do with the well-known transverse Zeeman effect). This new linearly polarized spectrum of the Sun is commonly referred to as the "second solar spectrum" (Stenflo & Keller 1996, 1997). It is richly structured with signatures of different kinds of scattering processes taking place in atomic systems of varying complexity. Of particular interest are the many often enigmatic signatures of quantum interference effects between fine structure states, hyperfine structure states, and magnetic substates (Hanle effect).

Atoms with non-zero electron spin S undergo fine structure splitting and exhibit J-state interference, whereas the atoms with non-zero nuclear spin I_s undergo hyperfine structure splitting (HFS) and show F-state interference. The Sc II 4247 Å line is governed by F-state interference.

Here we extend our previous work on the Ba II D_2 line (Smitha et al. 2013) to study the Sc II line at 4247 Å. This line arises due to the transition $J = 2 \rightarrow J = 2$. Due to coupling with the nuclear spin ($I_s = 7/2$), both the upper and the lower J levels are split into 5 F states each with 13 radiative transitions between them. The level diagram of this system is shown in Figure 1. We use the theory of F-state interference presented in Smitha et al. (2013, see also Smitha et al. 2012b), which takes account of the partial frequency redistribution (PRD) effects in the absence of magnetic fields. The results in the present paper do not include the contributions from magnetic fields. The theory of F-state interference in the presence of magnetic fields including the effects of PRD has been recently developed in Sowmya et al. (2014).

The 4247 Å line of Sc II is a chromospheric line with an approximate height of formation between 900–1100 km above the photosphere. ^{45}Sc is the only stable isotope of scandium. It shows prominent triple-peak structure in its Q/I spectra (see Gandorfer 2002; Stenflo 2003). Modeling of this triple-peak structure using the last scattering approximation was attempted by Belluzzi (2009). The effects of PRD and radiative transfer (RT) were neglected in that work.

In the present paper, by taking account of both PRD and RT effects, we study the sensitivity of the (I, Q/I) profiles to different atomic and atmospheric parameters. From our efforts we find it difficult to reproduce the triple-peak structure in Q/I and also the rest intensity.

The rest intensity is dependent on the model atmospheric properties. A plausible reason for the failure of reproducing the rest intensity is the use of one-dimensional (1D) model atmospheres. In several earlier works, such as Holzreuter & Stenflo (2007), Shapiro et al. (2011), Smitha et al. (2013), and Supriya et al. (2014), difficulties with the 1D models were encountered. The limitations of the 1D model atmospheres are also described in Kurucz (1997), Rutten (2002), and Uitenbroek & Criscuoli (2011). We believe that the three-dimensional model atmospheres may improve the fit to the observed rest intensity in case of the Sc II 4247 Å line.

In Q/I, the central peak is suppressed due to depolarization from HFS. However, the PRD peaks and the near wing continuum in the theoretical profiles match closely with the observed profiles. Our tests suggest that the observed Q/I profiles cannot be reproduced by modifications in the existing 1D standard model atmospheres. Hence we suspect the role of other physical effects in shaping the observed profiles, which may not have been accounted for in the present treatment. The lower level Hanle effect could qualify as being one such effect which can increase the polarization of the central peak, but its contribution is significant only for fields $\leqslant$1G (Belluzzi 2009).

The details of the various tests conducted by us are discussed in the sections below.

2. COMPUTING THE THEORETICAL PROFILES

The details of computing the Stokes profiles with F-state interference including the effects of PRD and RT using realistic

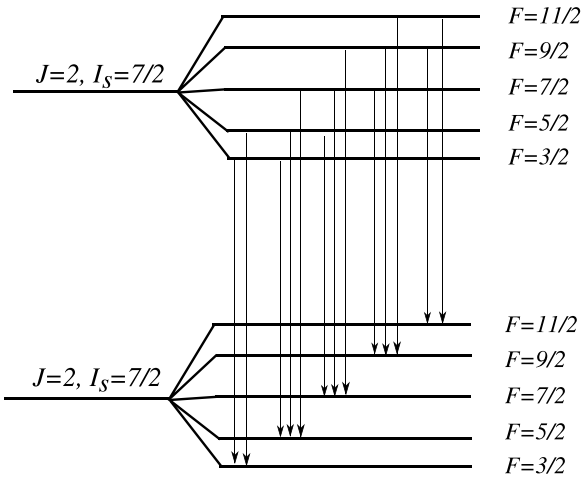

Figure 1. Level diagram showing the hyperfine structure splitting of the $3d4s$ and $3d4p$ atomic levels of the Sc II atom.

1D model atmospheres are presented in Smitha et al. (2013). We use the same here, too, and hence do not repeat them. However, certain physical quantities need to be redefined to represent the Sc II 4247 Å line system, and they are presented below.

The Voigt profile function: For the case of Sc II 4247 Å line, the Voigt profile function defined in Equation (3) of Smitha et al. (2013) is to be replaced by

$$\phi(\lambda, z) = \left[\frac{1}{25}\phi(\lambda_{33}, z) + \frac{3}{50}\phi(\lambda_{35}, z) + \frac{3}{50}\phi(\lambda_{53}, z) + \frac{1}{1400}\phi(\lambda_{55}, z) + \frac{5}{56}\phi(\lambda_{57}, z) + \frac{5}{56}\phi(\lambda_{75}, z) + \frac{2}{105}\phi(\lambda_{77}, z) + \frac{11}{120}\phi(\lambda_{79}, z) + \frac{11}{120}\phi(\lambda_{97}, z) + \frac{25}{264}\phi(\lambda_{99}, z) + \frac{7}{110}\phi(\lambda_{911}, z) + \frac{7}{110}\phi(\lambda_{119}, z) + \frac{13}{55}\phi(\lambda_{1111}, z)\right], \quad (1)$$

where $\phi(\lambda_{F_a F_b}, z)$ is the Voigt profile function for the $F_a \rightarrow F_b$ transition with F_a and F_b being the initial and excited F states, respectively. For notational brevity, the subscripts F_a and F_b in the ϕ terms are multiplied by 2 in the above equation.

The depolarizing elastic collision rate $D^{(2)}$: The branching ratios which describe the contribution from type-II and collisional redistribution (type-III) are defined in Equation (7) of Smitha et al. (2013). The depolarizing elastic collision rate $D^{(2)}$ which enter through the branching ratio $B^{(2)}$ can be computed using Equation (7.102) of Landi Degl'Innocenti & Landolfi (2004)

$$D^{(K)}(J) = C_E^{(0)}(J) - C_E^{(K)}(J), \quad (2)$$

where $C_E^{(K)}(J)$ is given by

$$C_E^{(K)}(J) = (-1)^K \frac{\begin{Bmatrix} J & J & K \\ J & J & \tilde{K} \end{Bmatrix}}{\begin{Bmatrix} J & J & 0 \\ J & J & \tilde{K} \end{Bmatrix}} C_E^{(0)}(J), \quad (3)$$

with $C_E^{(0)}(J) = \Gamma_E/(2J+1)$.

If the interaction between the atom and the colliding particle is assumed to be of dipolar type, then $\tilde{K} = 1$. In this case, $D^{(2)}(J) = 0.1\,\Gamma_E$. If the interaction is assumed to be dipole-dipole in nature, then $\tilde{K} = 2$. In this case, $D^{(2)}(J) = 0.243\,\Gamma_E$. We have tested that both these values of $D^{(2)}$ give nearly identical emergent Q/I profiles. This is because the Sc II 4247 Å line is formed at a height of 900–1100 km above the photosphere. This can be seen from Figure 2, where the intensity contribution functions C_I are plotted as a function of height using different FAL model atmospheres at line center wavelength. The temperature structures of the FAL models as a function of height is shown in Figure 3(a) (see Section 4.1 for a discussion on these models). The function C_I is defined as (see Stenflo 1994; Fluri & Stenflo 1999)

$$C_I(\tau, \mu) = \frac{1}{\mu} S_I(\tau, \mu)\, e^{-\tau/\mu}, \quad (4)$$

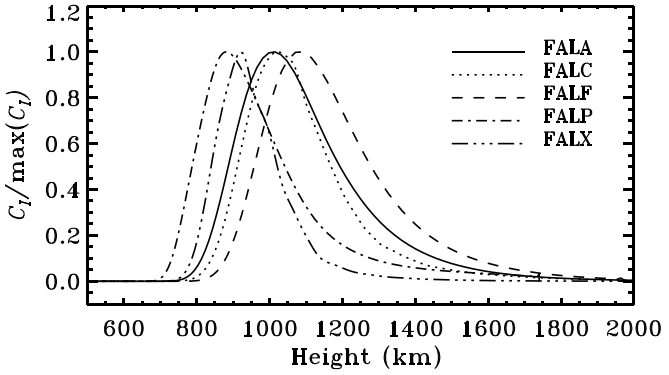

Figure 2. Contribution function C_I computed from the FAL model atmospheres at $\mu = 0.1$, for the line center wavelength.

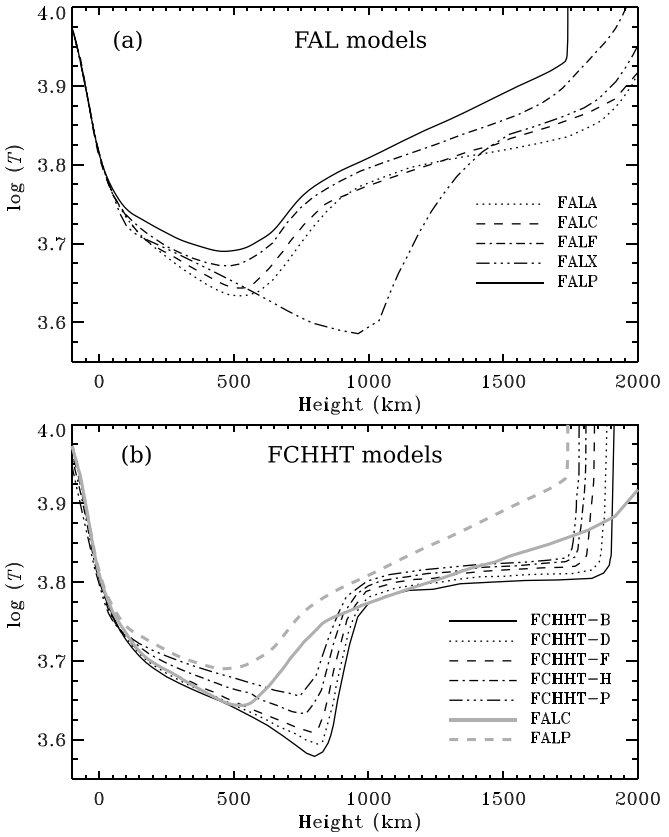

Figure 3. Temperature structures of the FAL and FCHHT model atmospheres.

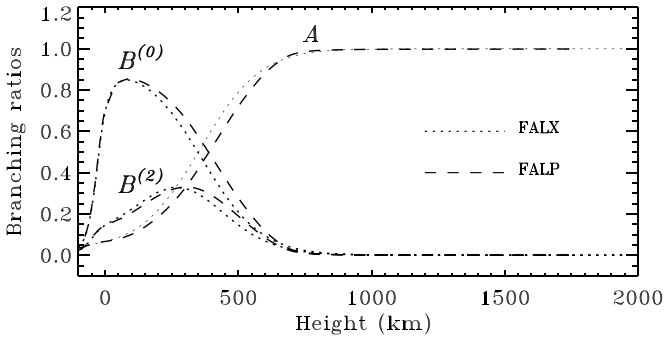

Figure 4. Branching ratios A and $B^{(K)}$, with $K = 0$ and 2, as a function of height computed using the FALX and FALP model atmospheres.

with $d\tau = -k_l dz$, k_l is the line absorption coefficient, and

$$I_\lambda(\mu, z = \infty) = \int_{-\infty}^{\infty} C_I(z', \mu) dz'. \quad (5)$$

From Equation (4), the contribution function is proportional to the source function S_I. Since S_I differs for each model atmosphere, the contribution functions also differ. However, the maximum contributions from the FAL model atmospheres fall within the height range 900–1100 km.

At these heights, the branching ratio $B^{(2)}$ is nearly zero as seen from Figure 4. We choose $D^{(2)}(J) = 0.243\,\Gamma_E$ for further computations.

3. OBSERVATIONS

The observations of the Sc II 4247 Å line analyzed in this paper were recorded on 2012 September 15 at IRSOL, Switzerland using the ZIMPOL-3 imaging polarimeter (Ramelli et al. 2010). The photoelastic modulator followed by a linear polarizer (beam splitter) was used as the polarization analyzer.

Though the telescope is almost free from instrumental polarization and cross talk effects around the equinox, to minimize residual instrumental signatures, a glass compensation plate was inserted in the optical path between the calibration optics and the analyzer. This also reduces the residual linear polarization offset. The optics was adjusted such that the positive Q represents the linear polarization parallel to the spectrograph slit. An image derotator (Dove prism) placed between the analyzer and the slit-jaw allowed us to rotate the solar image, and compensate for the solar rotation. The analyzer and the calibration optics were also rotated correspondingly. The observations were performed at a quiet region with the spectrograph slit placed parallel to the solar east limb. The spectrograph grating angle and a prefilter were selected to work with the thirteenth spectral order. On the CCD we got a resolution of 1.″44 per pixel along the spatial direction and 5.25 mÅ per pixel along the spectral direction. Three measurements were obtained by placing the slit at 5″, 15 ″, and 25″ from the solar limb. The observations at each μ position consisted of a sum of 1000 frames obtained with an exposure of 1 s, making the total exposure time as 16 minutes. The image motion perpendicular to the limb was compensated with a glass tilt-plate. The tilt of the plate was determined automatically with a limb recognition software using the information in the slit jaw image. The Stokes $(I, Q/I)$ images shown in Figure 5 were obtained after the data reduction. We also did a flat-field recording by moving the telescope around the disk center while recording 20 frames. The flat-field observations were used to correct the intensity images.

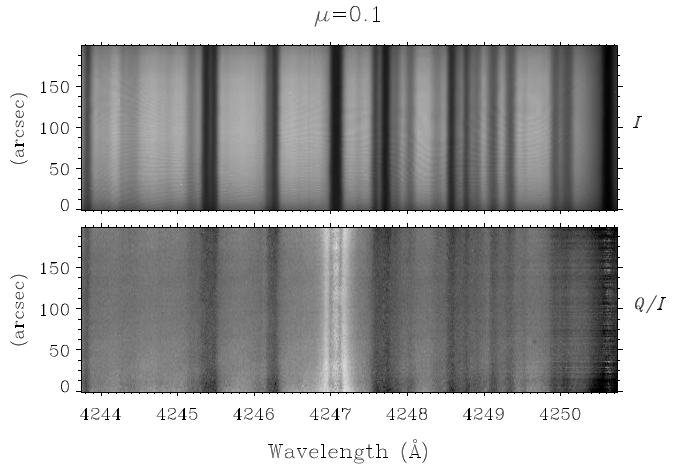

Figure 5. CCD image showing $(I, Q/I)$ for the Sc II 4247 Å line recorded on 2012 September 15 using the ZIMPOL spectropolarimeter at IRSOL, Switzerland.

The observed $(I, Q/I)$ profiles used in this paper were obtained after performing a spatial averaging from 60″ to 140″ along the slit.

3.1. Determining the Absolute Zero Level of Polarization

The absolute zero level of polarization is determined using the blend lines as described in Stenflo (2005, see also Stenflo et al. 1998). According to this method, the relative line depths of the depolarizing blend lines in Stokes I and Q/I are related with the following one-parameter model as

$$\left(\frac{p_c - p}{p_c}\right) = \left(\frac{I_c - I}{I_c}\right)^{\alpha}, \quad (6)$$

where I_c and p_c are the intensity and polarization of the continuum, and I and p are the respective quantities for the blend lines. α is a free model parameter that determines the shape of the depolarizing lines. We choose $\alpha = 0.6$ for further analysis. Figure 6 shows the comparison between the observed profile (solid line) and the profile computed using Equation ((6), second panel: dotted line). This dotted line represents $p_c[1 - (1 - (I/I_c))^{0.6}] - p_0$. Here p_0 is a free model parameter that represents the apparent level of the true zero point of the polarization scale. The blend line depth is sensitive to the value of p_c. To get the observed line depths, we need $p_c = 0.15\%$ ($p_{c,\mathrm{obs}}$). Also, to match the solid and the dotted profiles a shift of $p_0 = 0.07\%$ has to be applied. As seen from this figure, we obtain a good match between the solid and the dotted profiles for this set of parameters.

3.2. Stray Light Correction

Next, we applied a stray light correction of 2% of the continuum to both I and Q/I. For correcting the Q/I profile, we have used the value of p_c determined above. The details of the steps followed are given in Supriya et al. (2014). The comparison between the observed profiles with stray light correction (dashed line) and without (solid line) is shown in Figure 6. The stray light corrected observed profiles nearly overlap with the profiles without this correction.

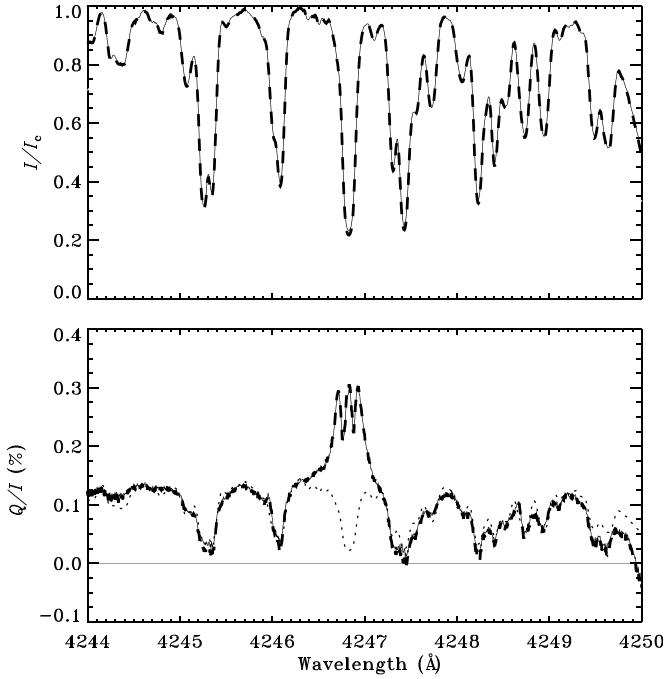

Figure 6. Fit to the blend lines around the Sc II 4247 Å line profile using Equation (6). The solid lines represent the observations, and dotted line in the second panel represents $p_c[1-(1-(I/I_c))^{0.6}]-p_0$. To obtain a fit, we choose $p_c = 0.15\%$ and $p_0 = 0.07\%$. The dashed lines show the observed profiles corrected for 2% stray light. The dashed and solid lines nearly overlap.

4. COMPARING THE THEORETICAL AND THE OBSERVED STOKES PROFILES

We compute the theoretical Stokes profiles using a procedure similar to the one described in Holzreuter et al. (2005, see also Anusha et al. 2011; Smitha et al. 2012a, 2013). We use the PRD-capable Multi-level Approximate Lambda Iteration code developed by Uitenbroek (2001, referred to as the RH-code) to compute the opacities, collision rates and intensity. These quantities are then given as inputs to the polarized RT equation defined in Equation (1) of Smitha et al. (2013). The expressions used to compute quantities such as the line and continuum source vectors, and their sum are same as Equations (5), (9), and (4) of Smitha et al. (2013). The Stokes profiles are computed by solving the transfer equation perturbatively (see Faurobert 1987; Nagendra et al. 2002).

The Sc II atom model, which is used as an input to the RH-code, is constructed with 8 J-levels coupled by 6 line transitions and 10 continuum transitions. The main line is treated in PRD and the others are treated under the assumption of complete frequency redistribution (CRD). The angle averaged redistribution functions of Hummer (1962) are used for intensity computations and the angle-averaged redistribution matrix presented in Smitha et al. (2013) is used for computing the polarization. The continuum is computed by assuming frequency coherent scattering and its expression is given in Equation (9) of Smitha et al. (2013). In the RH-code, all the blend lines are assumed to be depolarizing and are treated under LTE.

We compare the observed and the theoretical profiles computed using several model atmospheres and this is discussed in detail below.

4.1. FAL Models

The FAL realistic 1D model atmospheres are taken from Fontenla et al. (1993; FALA, FALC, FALF, and FALP models) and Avrett (1995; FALX model). Figure 3(a) shows their temperature structures as a function of height. The theoretical $(I, Q/I)$ profiles computed using the FAL models are shown in Figure 7. We have used the experimentally determined HFS constants given in Table 1 to calculate the energies of the F states. The profiles in this figure are smeared using a Gaussian with FWHM = 80 mÅ. This smearing contains contributions from both instrument and macroturbulent velocity fields. Instrumental broadening is about 40 mÅ. The rest corresponds to a macroturbulent velocity of 2.9 km s^{-1}.

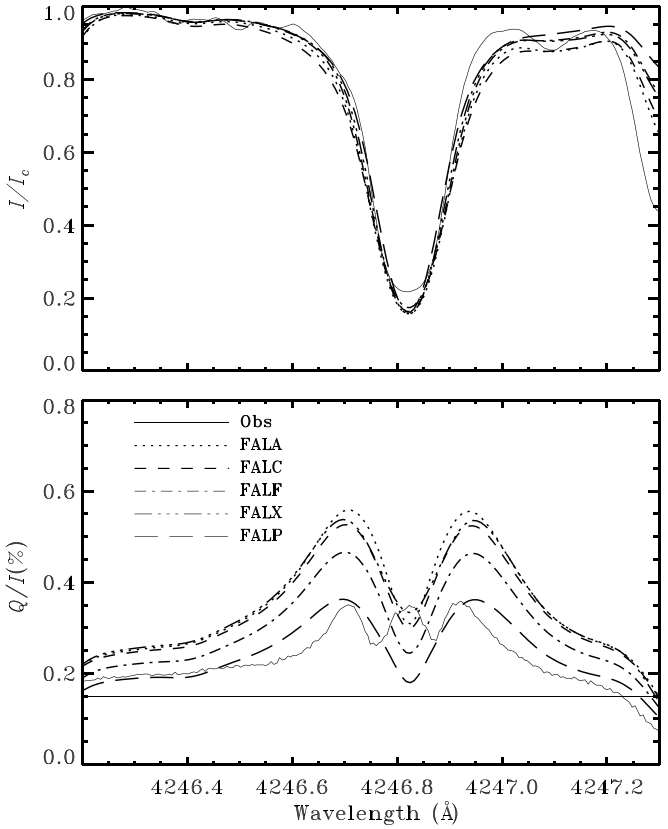

Figure 7. Theoretical $(I, Q/I)$ profiles from the five standard FAL model atmospheres.

Table 1
HFS Constants in MHz

Level	Experiment		Theory	
	A	B	A	B
Lower	128.2(8)	−39(11)	146.8	−25.5
Upper	215.7(8)	18(7)	202.5	−10.8

Upon comparing the theoretical and observed profiles, it is evident that our present treatment cannot provide an exact match to (1) the rest intensity, (2) the triple-peak structure in Q/I, and (3) the continuum polarization.

The theoretical intensity profiles are deeper than the observed profile and the values of rest intensity do not show much sensitivity to the variation in the model atmospheres within the FAL set. The theoretical Q/I profiles do not show the triple-peak structure for any of the FAL model atmospheres, whereas the observed Q/I profile shows prominent triple-peak structure.

The values of the continuum polarization ($p_{c,th}$) from the FAL models are greater than the value determined using the blend lines (Section 3.1). Such a discrepancy between $p_{c,th}$ and $p_{c,\mathrm{obs}}$ has been studied in detail by Stenflo (2005). In that paper, the

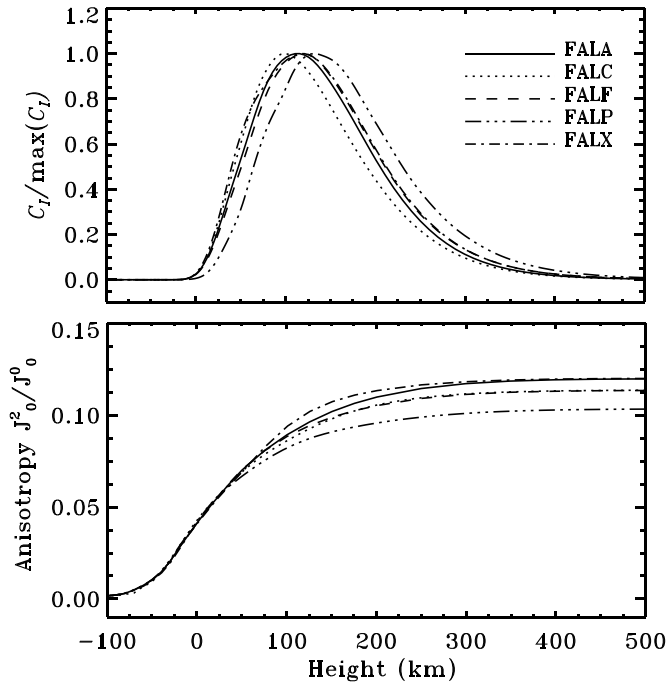

Figure 8. Contribution functions and anisotropy factors at a continuum wavelength plotted as a function of height for several FAL model atmospheres.

Table 2
Continuum Polarization from FAL and FCHHT Models

Atmosphere	$p_{c,th}$ (%)	Atmosphere	$p_{c,th}$ (%)
FALP	0.16	FCHHT-P	0.19
FALF	0.19	FCHHT-H	0.22
FALC	0.21	FCHHT-F	0.23
FALA	0.21	FCHHT-D	0.24
FALX	0.22	FCHHT-B	0.25

author points out that for $\lambda > 4000$ Å, the $p_{c,th} > p_{c,\mathrm{obs}}$ (see Figure 6 of Stenflo 2005). We also note that a similar problem with $p_{c,th}$ and $p_{c,\mathrm{obs}}$ was encountered while modeling the Cr I triplet around 5206 Å in Smitha et al. (2012a), and the model atmosphere FALF had to be modified in the deeper layers of the atmosphere, where the continuum is formed, to fit the $p_{c,\mathrm{obs}}$. Here, too, we face a similar problem. Among FAL models, the hotter the model atmosphere, the smaller is the value of $p_{c,th}$. This is because, as seen from Figure 3(a), the hotter models have smaller temperature gradients between 0–200 km, which leads to smaller anisotropy. The height of continuum formation can be obtained using the contribution functions shown in Figure 8. In the bottom panel of this figure, we have plotted the anisotropy factor J^2_0/J^0_0 (defined, for instance, in Holzreuter et al. 2005) at a continuum wavelength as a function of height. Among the FAL models, the FALP model gives the smallest anisotropy for the continuum. This results in smaller values of $p_{c,th}$. The values of $p_{c,th}$ computed from the FAL models are given in Table 2.

The difficulties in reproducing the observed Stokes profiles can originate from various sources such as an incorrect choice of model atmosphere, multidimensional RT effects, an incomplete treatment of atomic physics, etc. To shed light on these issues, we now try to model the observed profiles using another set of models with temperature structures different from the FAL models.

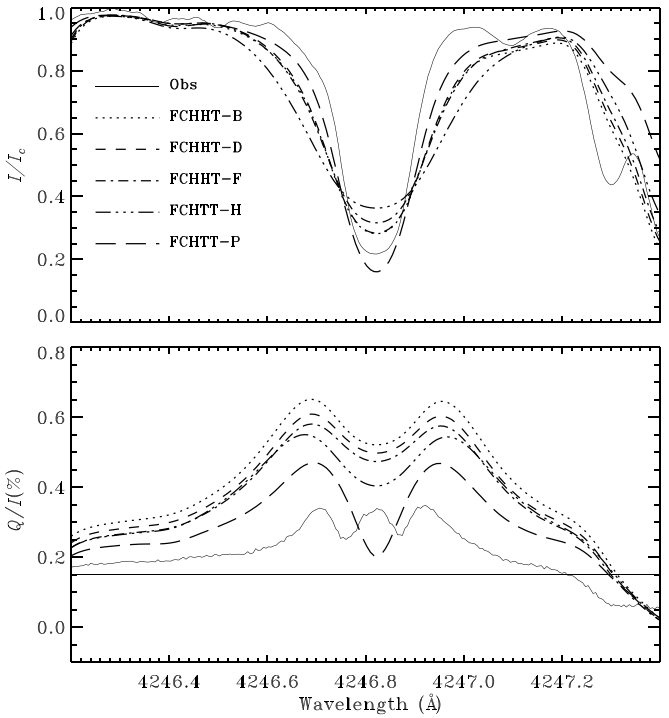

Figure 9. Stokes (I, Q/I) profiles of the Sc II 4247 Å line computed using the FCHHT models.

4.2. FCHHT Models

The FCHHT models are the updated models published by Fontenla et al. (2009). The temperature structures of these models as a function of height are shown in Figure 3(b). For comparison, the temperature structures of the FALC and FALP models are also shown. As seen from this figure, the temperature gradient in the FCHHT models are similar to the FAL models up to 500 km and then vary from the FAL models. Among the FCHHT models, the P model has the least temperature gradient which also is the hottest model. The B model, has the largest gradient and is also the coolest. In the height range 0–500 km, among the FAL models, it is the FALP model which has the least gradient, and this gradient is smaller than the FCHHT-P model too. A comparison between the FAL and FCHHT models is also presented in Rutten & Uitenbroek (2012).

The (I, Q/I) profiles computed from the FCHHT models are shown in Figure 9. We find that the updated models, too, fail to reproduce the observed Stokes profiles. We continue to face difficulties in reproducing the rest intensity, triple-peak structure in Q/I, and continuum polarization. We discuss each of these issues in the sections below.

4.2.1. Intensity Profile

In addition to a mismatch in line depth, the intensity profiles from the FCHHT models are wider than the observed profile. The FCHHT-B, D, F, and H models produce intensity profiles wider and shallower than the observed profile whereas the FCHHT-P model, produces profile deeper than the observed one. Hence in principle it should be possible to construct a two-component model, like the one described in Holzreuter et al. (2006), by mixing two appropriate models to get the required rest intensity. However, such a fit would give an intensity profile that is much too wide. There also could be a role of multidimensional RT effects in shaping the intensity profiles. However, the scope

of the present paper is restricted to 1D models only. Therefore, it is difficult to quantify to what extent the multidimensional effects play a role.

4.2.2. Central Peak in Q/I Profile

The FCHHT models have different temperature gradients in the upper chromospheric layers, where the line is formed, compared to the FAL models. However, this is of little help in improving the fit to the triple-peak structure in Q/I. Hence, the failure of both FAL and FCHHT models, with very different temperature structures, and the fact that the central peak is mostly governed by the F-state interference effects, indicates that the mismatch at the central peak in Q/I is originating from an incomplete treatment of atomic physics. An effect not accounted for in our treatment is the lower-level Hanle effect. Belluzzi (2009) showed that this effect can increase the amplitude of the central peak in Q/I when the magnetic field strength, $B \approx 1$G.

4.2.3. Continuum Polarization

The $p_{c,th}$ from the FCHHT models are similar in magnitude to the ones predicted by the FAL models. Among FCHHT models, the warmer model, FCHHT-P, predicts smaller $p_{c,th}$. For this reason, the FCHHT-P model provides a better fit to the PRD peaks when compared to other FCHHT models. However, this fit is not better than the one obtained from FALP model. The values of $p_{c,th}$ from FCHHT models are given in Table 2. Once again, none of these values match with $p_{c,\mathrm{obs}}$.

The FALP and FCHHT-P models, though represent faculae conditions, provide better fits to the PRD wing peaks and continuum because of the above stated reasons. Hence, in the sections below we conduct a few more tests using the FALP model atmosphere and vary some of the atomic parameters. Note that in all the figures, the horizontal thin solid line in Q/I represents the value of $p_{c,\mathrm{obs}}$.

4.2.4. Effect of Macro and Micro-turbulent Velocities

Figure 9 shows that the intensity profiles computed from the FCHHT models are wide compared to the observed profile. Both macro and micro-turbulent velocities influence the width of the intensity profiles. Reducing the macroturbulence leads to a decrease in the smearwidth. In the top two panels of Figure 10, we show a comparison between the Stokes profiles computed using a smearwidth of 80 mÅ ($V_{\mathrm{turb-ma}} = 2.9$ km s^{-1}) and 40 mÅ ($V_{\mathrm{turb-ma}} = 0$ km s^{-1}). In the case of the 4247 Å line we do not see a significant variation in (I, Q/I) with the variation in smearwidth. However, upon reducing the micro-turbulent velocity ($V_{\mathrm{turb-mi}}$) by a constant factor (1.5 and 4.0), we see that the width of the intensity profile decreases significantly. This is shown in the bottom two panels of Figure 10. In addition, the central dip in Q/I gets deeper. Thus, it is not possible to improve the fit to the observed profile by varying the turbulent velocity.

4.3. Studying the Sensitivity of the (I, Q/I) Profiles

We now study the response of the Stokes profiles by varying a few atomic parameters. We note that in some of these tests, we do recover the triple-peak structure in Q/I. However, the modifications made to the atomic parameters are artificial and are done only for the purpose of demonstrating the sensitivity of the Stokes profiles on these parameters (see Figures 11–13).

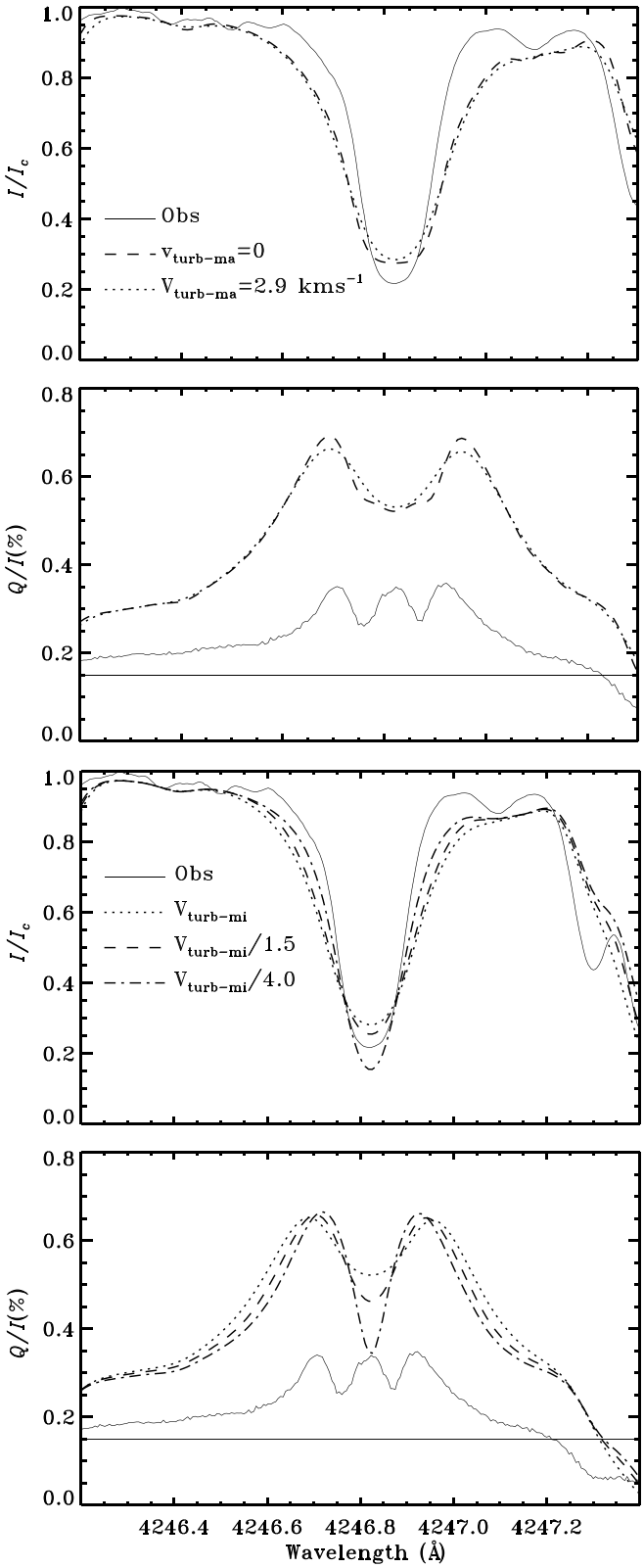

Figure 10. Stokes (I, Q/I) profiles of the Sc II 4247 Å line computed by varying the macroturbulent ($V_{\mathrm{turb-ma}}$) velocity in the top two panels and micro-turbulent velocity ($V_{\mathrm{turb-mi}}$) in the bottom two panels. Model atmosphere used is FCHHT-B.

These tests also demonstrate that the principle of spectroscopic stability is being satisfied, which proves the correctness of our treatment. Since the intensity profiles do not show much sensitivity to these tests, we only show the Q/I profiles.

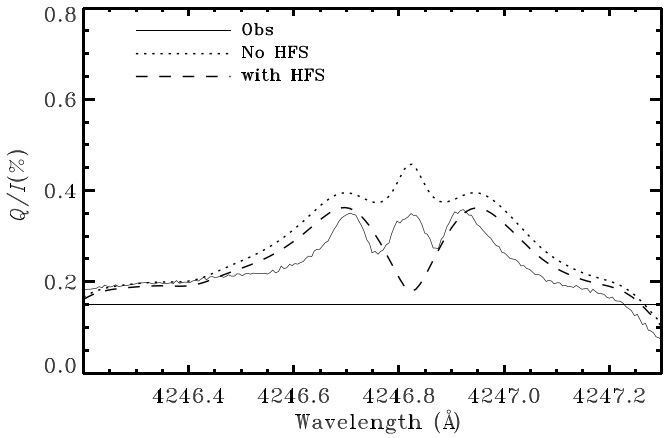

Figure 11. Q/I profiles computed with and without hyperfine structure splitting.

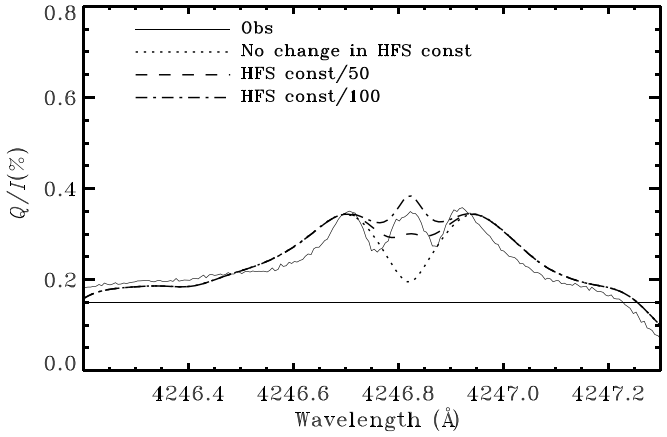

Figure 12. Q/I profiles computed by reducing the HFS constants of the upper level by factors of 50 and 100.

4.3.1. Effects of F-state Interference

It is well known that the decoherence caused by the HFS of the J states leads to a depolarization in the core of the Q/I line profile. In case of the Sc II 4247 Å line, the splitting between them is quite large and hence the decoherence. This leads to an enhanced depolarization in the line core, resulting in a fully suppressed central peak. When the nuclear spin $I_s = 0$, we recover the triple-peak structure in Q/I as demanded by the principle of spectroscopic stability (Stenflo 1994). Figure 11 shows the comparison between the profiles with and without HFS.

To better understand the large depolarization, we try to compare the F-state splitting with the radiative widths of the upper levels. We recall that, in our treatment, the lower levels are assumed to be infinitely sharp and hence do not interfere. The interfering upper F states, the splitting between them, and the ratio (Ω) between the splitting and the radiative width are given in Table 3, where the Einstein A co-efficient is taken as 1.29×10^8 s^{-1}.

We know that when Ω is close to unity, the splitting sensitivity is maximum. However, in case of the Sc II 4247 Å line system, we see from Table 3 that Ω is much greater than one. This partly explains the large depolarization in Q/I at the line center. When the HFS constants are rescaled by a factor of 50 or 100, such that Ω approaches unity, the central peak rises up. This again is a proof of the principle of spectroscopic stability

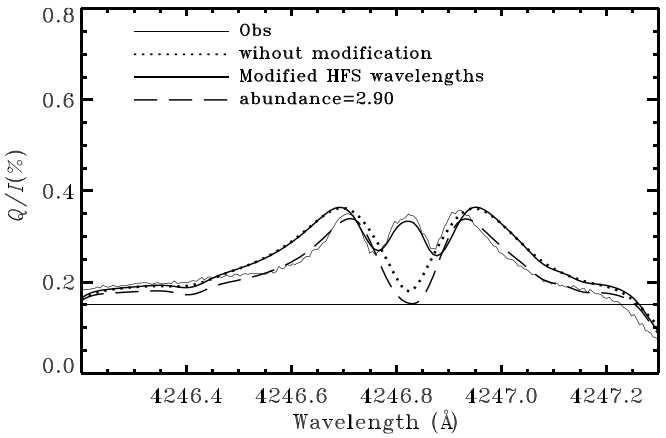

Figure 13. Q/I profiles computed by modifying one of the HFS wavelengths and by modifying the abundance of Sc.

Table 3
Comparison between the F-state Splitting and Their Radiative Widths

F_{u1}	F_{u2}	ΔE (Hz)	$s = (\Delta\lambda)_F$ (mÅ)	Ω
3/2	5/2	5.3121×10^8	2.605	25.874
3/2	7/2	1.27941×10^9	6.274	62.296
3/2	9/2	2.24910×10^9	11.029	109.542
3/2	11/2	3.44605×10^9	16.89	167.844
5/2	7/2	7.48200×10^8	3.669	36.442
5/2	9/2	1.71788×10^9	8.424	83.672
5/2	11/2	2.91484×10^9	14.293	141.972
7/2	9/2	9.69685×10^8	4.755	47.230
7/2	11/2	2.16664×10^9	10.624	105.518
9/2	11/2	1.19695×10^9	5.869	58.297

being satisfied. These profiles are shown in Figure 12. Rescaling the HFS constants reduces the splitting between F states and hence the decoherence.

Also, as seen from Equation (1) the $F_b = 11/2 \rightarrow F_a = 11/2$ is the strongest transition and it has maximum coupling with the $F_b = 9/2 \rightarrow F_a = 11/2$ transition. In other words, the shape of the emergent Q/I profile is controlled mainly by these transitions and the interference between their upper levels. When the HFS wavelengths of these two transitions are set equal to each other, we recover the central peak in Q/I as shown in Figure 13. Such a modification, once again, reduces the decoherence and hence the depolarization.

One can notice from Figure 13 that the width of theoretical Q/I profile and the amplitude of the PRD peaks are larger than in the observed profile. Both of these are sensitive to the solar abundance of Sc. Zhang et al. (2008) discuss the uncertainty in the abundance value of Sc in the Sun. Their study is based on modeling the observed intensity profiles of different Sc lines. They find that different abundances are needed to fit different lines and conclude that the abundance value is 3.07 ± 0.04. The long dashed line in Figure 13 is the profile computed with an abundance of 2.90. With this reduced abundance, the fit to the PRD peaks and the near wing continuum in the Q/I profile improves.

4.3.2. Collisions

In addition to the HFS, collisions can significantly modify the line core polarization of the observed profiles. The

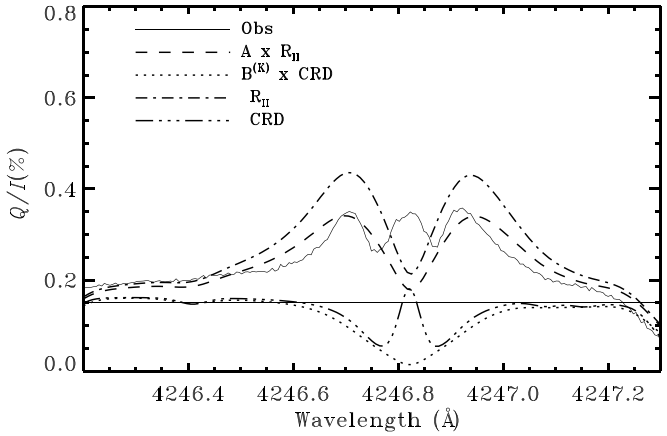

Figure 14. Contributions to the Q/I profile from type-II frequency redistribution and CRD. The profiles before and after multiplying the branching ratios are shown.

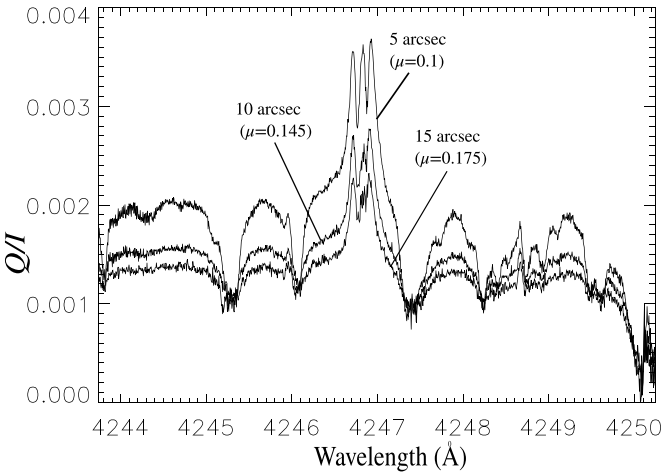

Figure 15. Q/I profiles of Sc II 4247 Å line observed at different limb distances.

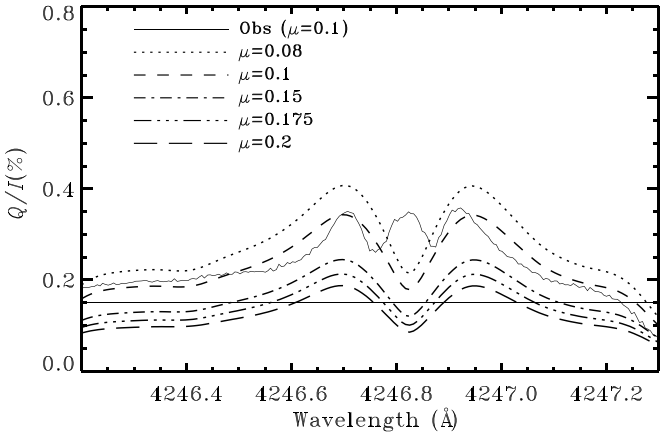

Figure 16. Theoretical Q/I profiles computed at various limb distances.

contribution from collisional redistribution depends on the branching ratio B. In case of the Sc II 4247 Å line, this contribution is insignificant. Figure 14 shows the individual contributions from type-II frequency redistribution and CRD, with their corresponding branching ratios being multiplied. We note that in our computations the type-III redistribution has been replaced with CRD like in Smitha et al. (2012a, 2013) to reduce the computing time. This replacement does not affect the Stokes profiles.

The variation of the branching ratios A and $B^{(K)}$ as a function of height in the atmosphere for the FALP model is shown in Figure 4. $B^{(K)}$ takes a value close to zero at higher layers in the atmosphere. Since the Sc II 4247 Å line is formed in the upper chromosphere, the contribution to the line center is primarily from type-II redistribution. The Q/I profile $B^{(K)}\times$ CRD goes nearly to zero at the line center (dotted line in Figure 14). Thus, we can exclude the possibility that an approximate treatment of collisions might be contributing to the difficulties in reproducing the Q/I central peak.

Figure 14 also shows the Q/I profiles computed with type-II redistribution and CRD alone (without A and $B^{(K)}$ multiplied). The two side peaks on either side of the central peak are formed due to PRD and can be reproduced only by type-II redistribution. CRD alone cannot reproduce them. Thus, a proper account of PRD is essential to model this line.

4.3.3. Variation in μ

The observed profiles studied till now were recorded at a limb distance $\mu = 0.1$. When the line profiles were observed at nearby μ positions, they showed a large variation in the polarization of the central peak. These profiles are shown in Figure 15. At $\mu = 0.145, 0.175$, the central peak is depolarized and only the two PRD side peaks stand out. The larger CLV of the central peak as compared with the side peaks is to be expected from spatially varying magnetic fields, since the Hanle effect can only operate in the Doppler line core but not in the wings. This behavior is supported by the observed spatial fluctuations along the spectrograph slit: we find the line core amplitude of Q/I to vary much more than the side peaks. In contrast, the theoretical profiles computed for different μ values in the absence of magnetic fields (see Figure 16) do not show a variation of this kind.

There are therefore strong reasons to believe that the line core is greatly influenced by magnetic fields via the Hanle effect. This influence is normally in the form of depolarization, reduction of the polarization in the core. However, the Hanle effect may also go in the opposite direction when the atomic polarization in the lower level is considered, as found by Belluzzi (2009) for fields of order 1 G. It therefore remains a possibility that the observed Q/I central peak that we are unable to reproduce with our non-magnetic modeling could be due to the Hanle effect in the lower atomic level.

5. CONCLUSIONS

In this paper, we have tried to study the Sc II 4247 Å line, the polarization profiles of which are governed by the F-state interference effects. The observations, used by us, were taken at IRSOL using ZIMPOL 3 polarimeter in 2012 September in a quiet region near the solar limb.

Due to its large nuclear spin, the upper and lower J-levels split into 5 F states each giving rise to 13 radiative transitions between them. The decoherence between the F states is quite large and the emergent polarization profiles are sensitive to the energy difference between the F states. We have investigated the sensitivity of the theoretical Stokes profiles, in the absence of magnetic fields, to different atmospheric and atomic parameters. All the 1D model atmospheres tried by us (FAL and FCHHT models) fail to reproduce the triple-peak structure in Q/I and also the rest intensity. Also, the continuum polarization predicted by all models, except FALP, is larger than the

observed value. The PRD peaks and the near wing continuum in the theoretical profiles match closely with the observed ones only for the FALP model, but this model represents faculae conditions. We also show that a proper treatment of PRD is essential to model this line, and CRD alone cannot reproduce the PRD peaks.

The intensity profiles computed from the FAL models match well with the observed profile except at the line center. In case of FCHHT models, both the line width and line depth of the theoretical profiles match poorly with the observations. It may be possible to improve the fit to the intensity profiles if multidimensional RT effects are taken into account.

The Q/I core peak is more sensitive to the variations in atomic parameters than the atmospheric parameters. Observations indicate that the central peak in Q/I is quite sensitive to the Hanle effect. There might be positive contributions from the magnetic field to the central peak polarization through the lower level Hanle effect for field strengths of order 1 G.

Thus, in spite of a detailed account of PRD, RT, and HFS effects we are unable to reproduce the central peak. All these results lead us to believe that there might be other physical effects, unaccounted for in our treatment, playing a role in shaping the Q/I profiles. One such effect is the mentioned lower-state Hanle effect, a possibility that needs to be explored in the future.

We acknowledge the use of HYDRA cluster facility at the Indian Institute of Astrophysics for computing the results presented in the paper. We are grateful to Dr. Han Uitenbroek for providing us with his realistic atmospheric modeling code. H.N.S. thanks Ms. H. D. Supriya for interesting discussions. Research at IRSOL is financially supported by State Secretariat for Education, Research and Innovation, SERI, Canton Ticino, the city of Locarno, the local municipalities, the foundation Aldo e Cele Daccò, and the Swiss National Science Foundation grant 200021-138016. R.R. acknowledges financial support by the Carlo e Albina Cavargna foundation. We thank the referee for useful comments and suggestions which helped improve the results presented in this paper.

REFERENCES

Anusha, L. S., Nagendra, K. N., Bianda, M., et al. 2011, ApJ, 737, 95
Avrett, E. H. 1995, in Infrared Tools for Solar Astrophysics: What's Next?, ed. J. R. Kuhn & M. J. Penn (Singapore: World Scientific), 303
Belluzzi, L. 2009, A&A, 508, 933
Faurobert, M. 1987, A&A, 178, 269
Fluri, D. M., & Stenflo, J. O. 1999, A&A, 341, 902
Fontenla, J. M., Avrett, E. H., & Loeser, R. 1993, ApJ, 406, 319
Fontenla, J. M., Curdt, W., Haberreiter, M., Harder, J., & Tian, H. 2009, ApJ, 707, 482
Gandorfer, A. 2002, The Second Solar Spectrum: A High Spectral Resolution Polarimetric Survey of Scattering Polarization at the Solar Limb in Graphical Representation. Volume II: 3910 Å to 4630 Å (Zurich: vdf Hochschulverlag)
Holzreuter, R., Fluri, D. M., & Stenflo, J. O. 2005, A&A, 434, 713
Holzreuter, R., Fluri, D. M., & Stenflo, J. O. 2006, A&A, 449, L41
Holzreuter, R., & Stenflo, J. O. 2007, A&A, 467, 695
Hummer, D. G. 1962, MNRAS, 125, 21
Kurucz, R. 1997, in Proc. IAU Colloq. 189, Fundamental Stellar Properties, ed. T. R. Bedding, A. J. Booth, & J. Davis (Dordrecht: Kluwer), 217
Landi Degl'Innocenti, E., & Landolfi, M. 2004, Polarization in Spectral Lines (Astrophysics and Space Science Library, Vol. 307; Dordrecht: Kluwer)
Nagendra, K. N., Frisch, H., & Faurobert, M. 2002, A&A, 395, 305
Ramelli, R., Balemi, S., Bianda, M., et al. 2010, Proc. SPIE, 7735, 77351Y
Rutten, R. J. 2002, JAD, 8, 8
Rutten, R. J., & Uitenbroek, H. 2012, A&A, 540, A86
Shapiro, A. I., Fluri, D. M., Berdyugina, S. V., Bianda, M., & Ramelli, R. 2011, A&A, 529, A139
Smitha, H. N., Nagendra, K. N., Stenflo, J. O., et al. 2012a, A&A, 541, A24
Smitha, H. N., Nagendra, K. N., Stenflo, J. O., & Sampoorna, M. 2013, ApJ, 768, 163
Smitha, H. N., Sowmya, K., Nagendra, K. N., Sampoorna, M., & Stenflo, J. O. 2012b, ApJ, 758, 112
Sowmya, K., Nagendra, K. N., Stenflo, J. O., & Sampoorna, M. 2014, ApJ, 786, 150
Stenflo, J. 1994, in Solar Magnetic Fields: Polarized Radiation Diagnostics (Astrophysics and Space Science Library, Vol. 189; Berlin: Springer), 385
Stenflo, J. O. 2003, in ASP Conf. Ser. 307, Solar Polarization, ed. J. Trujillo-Bueno & J. Sanchez Almeida (San Francisco, CA: ASP), 385
Stenflo, J. O. 2005, A&A, 429, 713
Stenflo, J. O., & Keller, C. U. 1996, Natur, 382, 588
Stenflo, J. O., & Keller, C. U. 1997, A&A, 321, 927
Stenflo, J. O., Keller, C. U., & Gandorfer, A. 1998, A&A, 329, 319
Supriya, H. D., Smitha, H. N., Nagendra, K. N., et al. 2014, ApJ, 793, 42
Uitenbroek, H. 2001, ApJ, 557, 389
Uitenbroek, H., & Criscuoli, S. 2011, ApJ, 736, 69
Zhang, H. W., Gehren, T., & Zhao, G. 2008, A&A, 481, 489